VOL. 12, NO. 4, FEBRUARY 2017 ISSN 1819-6608
ARPN Journal of Engineering and Applied Sciences

www.arpnjournals.com

TRANSONIC FLOW IN A CHANNEL WITH A CENTRAL BODY

A. N. Ryabinin and A. F. Suleymanov
Saint-Petersburg State University, St. Petersburg, Russia
E-Mail: a.ryabinin@spbu.ru

ABSTRACT

2D transonic flow in two channels of variable cross-section with a central body is studied numerically using solvers based on the Euler and Reynolds-averaged Navier-Stokes equations. Ansys CFX and SU^2 packages are used. The flow velocity is supersonic at inlets and outlets of channels. At small inflow Mach number between the supersonic regions, there is a local subsonic region. The increase in the Mach number leads to arising and expansion of supersonic regions and rapprochement. At the moment of coalescence of two regions the shock position abruptly changes. Computations reveal a hysteresis in the shock position versus the inflow Mach number. In the certain range of inlet Mach number, there are asymmetrical solutions of the equations.

Keywords: transonic flow, shock wave, instability, computational fluid dynamics, hysteresis.

INTRODUCTION

Shock wave instability study was carried out for the channel between two symmetrical wedges [1], two cylinders placed side by side and to the infinite chain of cylinders normally oriented to the flow velocity [2, 3]. In this cases, the instability and hysteresis caused by the existence of reflections of two types. In this paper we consider the different instability, associated with the interaction of supersonic regions.

It was demonstrated that the transonic flow near the airfoil with surface of small curvature is sensitive to the small change in free stream velocity [4-8]. Sensitivity can be explained by the interaction of local supersonic regions near the airfoil. Two supersonic regions exist near the surface of small curvature. The leading supersonic region is terminated by shock wave. Behind the shock the flow is subsonic. Behind subsonic line the flow is supersonic again. Increasing in the Mach number leads to arising of two supersonic regions. The distance between regions decreases. However, it could not be zero. At the moment of coalescence of two regions the shock position abruptly changes. Computations reveal a hysteresis in the shock position versus the inflow Mach number. A review of studies on this topic is published in [8].

Problems of the shock waves instability were studied in [9, 10] for the channels with wall break or bend.

FORMULATION OF THE PROBLEM AND NUMERICAL METHOD

We consider 2D flow in two channels with the central body. Straight segments constitute lower and upper walls of the channels. Both channels are diverging. There are central bodies of different shapes in the channels. The sketches of the channel are presented below in the Figure-1 and Figure-6.

First channel. Upper and lower walls:

$$\text{if } 0 \le x \le 1.3 \quad \text{then} \quad y = \pm 0.948 \pm 0.04x, \tag{1}$$

$$\text{if } 1.3 \le x \le 2.7 \quad \text{then} \quad y = \pm 1.0 \pm 0.229(x - 1.3). \tag{2}$$

Central body:

$$\text{if } 1.2 \le x \le 1.25 \quad \text{then} \quad y = \pm\sqrt{(x-1.25)^2 + 0.05^2}, \tag{3}$$

$$\text{if } 1.25 \le x \le 2.7 \quad \text{then} \quad y = \pm 0.05. \tag{4}$$

Second channel. Upper and lower walls:

$$\text{if } 0 \le x \le 2.3 \quad \text{then} \quad y = \pm 0.88 \pm 0.0521x, \tag{5}$$

$$\text{if } 2.3 \le x \le 3.0 \quad \text{then} \quad y = \pm 1.0 \pm 0.229(x - 2.3). \tag{6}$$

Central body:

$$\text{if } 1.4 < x \le 3.0 \quad \text{then} \quad y = \pm 0.001 \pm 0.119(x - 1.4), \tag{7}$$

$$\text{if } x = 1.4 \quad \text{then} \quad -0.01 < y < 0.01. \tag{8}$$

The coordinate (x, y) are dimensional. Here and further coordinates are given in meters. Inlet and outlet boundaries are vertical straight segments. Preliminary results of transonic flow study in the second channel were reported in [11].

2D unstructured (for inviscid fluid) or hybrids (for viscous fluid) mesh were generated using package Gmsh [12]. These meshes were used for calculations in the package Stanford University Unstructured (SU^2) [13]. A program written in Pascal language transformed them into 3D meshes, whose lateral size was equal to one element. The transformed meshes are in the TGrid/Fluent format [14], which is suitable for the calculation in the commercial package Ansys CFX [15]. In the solution of RANS equations, the mesh was fined near the walls. The non-dimensional thickness of the first mesh layer y^+ is less than 1 or greater than 30. In the second case, the wall functions are used. The vanishing flux of heat is used on the wall. The slip condition for Euler equations and no-slip condition for RANS equations are accepted. Specific heat of air at constant pressure is equal 1004.4 J / (kg K). Molar mass is equal to 28.96 kg/kmol.

FLOW CALCULATIONRESULTS FORTHE FIRST CHANNEL

The mesh for solution of Euler equations has 149,480 elements. Most of the solutions of Reynolds averaged Navier-Stokes (RANS) equations are obtained with the mesh with 119,011 elements. At the inflow boundary temperature T_{in} = 250 K, Mach number M_{in}, pressure p_{in} or Reynolds number Re for RANS equations on the base of the length of 1 m are set. Solutions of Euler

equations are obtained with both SU[2] and Ansys CFX finite volume solvers. Solutions of RANS equations are obtained with Ansys CFX. Reynolds number Re is equal to $3.5 \cdot 10^7$ or $3 \cdot 10^5$. The model of turbulence k-ω SST is used. Inflow turbulence intensity is equal to 5%.

Figure-1shows three patterns of Euler equations solutions at $M_{in} = 1.28$. White line corresponds M = 1. The first pattern a) has two supersonic regions divided by the subsonic one. In the second pattern b) supersonic regions coalesce near walls of the channel and form the single supersonic region. The third pattern shows coalescence of supersonic regions near the lower wall. In the upper part of the channel, the supersonic regions are divided by the subsonic region. In the lower part of the channel, there is the single supersonic region.

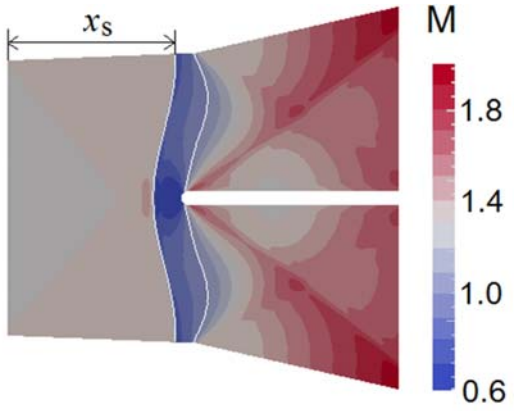

a)

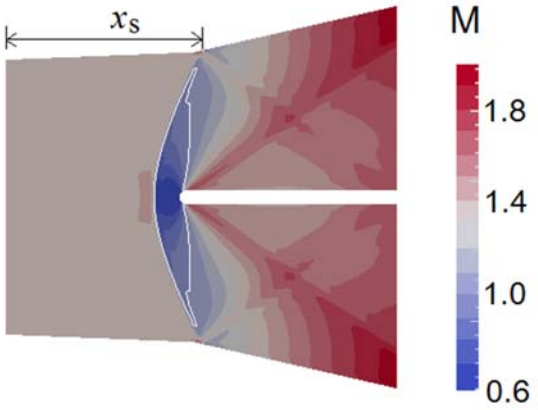

b)

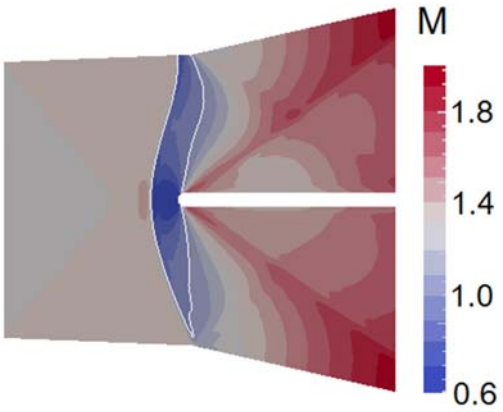

c)

Figure-1. Three patterns of shock wave configuration in the first channel for solutions of Euler equations. $M_{in} = 1.285$. Mach number distribution: a) two supersonic regions, b) single supersonic region, c) asymmetrical solution.

The fourth pattern of shock wave configuration is not presented in the Figure-1. The lower part of the channel includes two separated supersonic regions. There is coalescence of supersonic regions in the upper part of the channel.

The distance from the inflow boundary to shock wave near the wall is denoted by x_s, as it is shown in the Figure-1 a) and b). For asymmetrical solution the distances x_s in the upper and lower parts of the channel differ from one another.

If inflow Mach number $M_{in} < M_1$ then pattern with two supersonic regions is obtained. If $M_{in} > M_2$ then we receive pattern with the single supersonic region. In the range $M_1 \leq M_{in} \leq M_2$ two pattern can be realised. It depends on initial condition. If solution with two supersonic regions is taken as an initial condition then pattern with two supersonic regions is obtained. If solution with single supersonic regions is taken as an initial condition then pattern with single supersonic regions is obtained. Increasing in M_{in} from $M < M_1$ up to M_2 leads to realisation of pattern with two supersonic regions. At $M_{in} = M_2$ the flow pattern dramatically changes and distance x_s abruptly changes too. Supersonic regions coalesce. Pattern transforms to another one. Subsequent decreasing of M_{in} conserves the type of pattern down to $M_{in} = M_1$. At $M_{in} = M_1$ thepattern changes again. Therefore, we reveal hysteresis phenomenon.

Figure-2 demonstrates hysteresis obtained by two solvers. Both solvers show existence of hysteresis, but ranges of hysteresis slightly differ from one another.

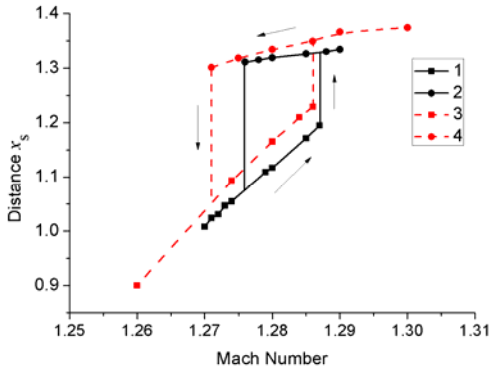

Figure-2. Distance x_s as a function of inflow Mach number M_{in} for first channel. Euler equations. 1, 2 - SU^2 solver, 3, 4 - Ansys CFX solver. 1, 3 - pattern with two supersonic regions, 2, 4 - pattern with the single region.

If solution of Euler equations at the angle of attack $\alpha \neq 0$ is taken as initial condition, the asymmetrical solution that corresponds pattern in the Figure-1 c) can be received. The range of inflow Mach number M_{in} that corresponds to existence of asymmetrical pattern is less than the range of hysteresis. In the Figure-3, there is the dependence of distance x_s on M_{in}. Dependence is obtained with Ansys CFX solver for solution of Euler equations. Two black lines in the Figure-3 correspond to different symmetrical patterns. Others two lines stand for asymmetrical patterns.

Hysteresis phenomenon can be formulated for aerodynamic force coefficient for central body.

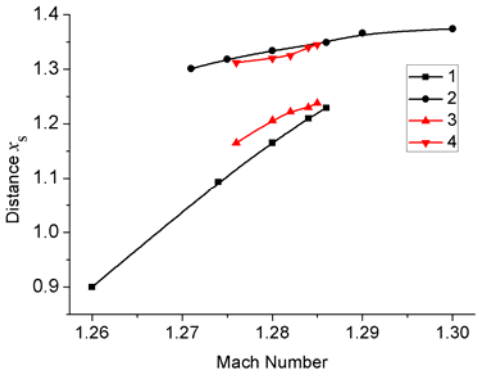

Figure-3. Dependence of distance x_s on inflow Mach number for the first channel: 1- pattern with two supersonic regions, 2 - pattern with single supersonic region, 3 - asymmetrical pattern.

In the Figure-4 dependence of drag coefficient C_D of central body on inflow Mach number M_{in} is shown. The dependence is obtained with Ansys CFX solver, v. 14. If M_{in} increases from $M < M_1$ up to M_2 then calculation reveals flow pattern with two supersonic regions. At $M_{in} = M_2$ pattern changes, but drag coefficient does not dramatically change. Subsequent decreasing of M_{in} does not change flow pattern with single supersonic regions until $M_{in} = M_1$. Further decreasing of M abruptly changes the flow pattern and drag coefficient. In the same graph there are values C_D for asymmetrical solutions of Euler equations.

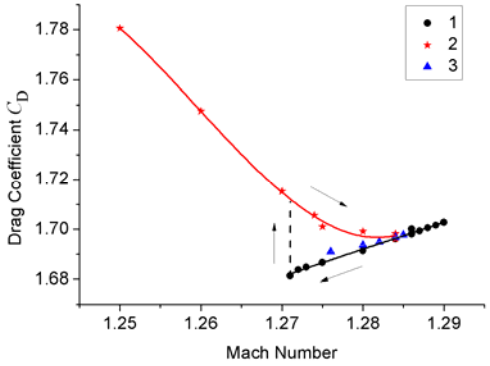

Figure-4. Dependence of drag coefficientC_D of central body in the first channel on inflow Mach number: 1- pattern with single supersonic region, 2- pattern with two supersonic regions, 3- asymmetrical pattern.

The relationship between the lift on a central body and its drag, expressed in terms of the dependence of the lift coefficient on the drag coefficient, is displayed in the diagram Figure-5. In the diagram, one can see four branches, whose flow patterns differ from one another. Two branches have common points.

Hysteresis range and the range of asymmetrical patterns for RANS equations differ from the ranges for Euler equations. For Reynolds number $Re = 3.5 \cdot 10^7$ hysteresis exists in the range $1.273 \leq M_{in} \leq 1.296$, the asymmetrical patterns are obtained at $1.284 \leq M_{in} \leq 1.296$. For $Re = 3 \cdot 10^5$ hysteresis range is observed at $1.296 \leq M_{in} \leq 1.306$. Asymmetrical patterns exist in the range of inflow Mach number $1.296 \leq M_{in} \leq 1.306$.

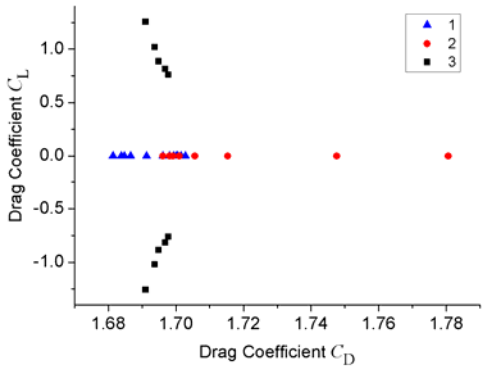

Figure-5. Four regimes of transonic flow in the first channel: 1- single supersonic regions, 2- two supersonic region, 3- asymmetrical regimes.

FLOW CALCULATION RESULTS FOR THE SECOND CHANNEL

The mesh for solution of Euler equations has 109,864 elements. Most of the solutions of Reynolds averaged Navier-Stokes (RANS) equations are obtained with the mesh with 120,786 elements. A few calculations are carried out with more fined mesh near walls with 125314 elements. Calculations demonstrate the independence of the results on mesh size.

On the inflow boundary temperature $T_{in} = 250$ K, Mach number M_{in}, pressure $p_{in} = 5 \cdot 10^4$ Pa or Reynolds number $Re = 3.4 \cdot 10^7$ for RANS equations on the base of the length of 1 m are set. A few calculations are performed at $Re = 5.6 \cdot 10^6$. Solutions of equations are obtained with both SU^2 and Ansys CFX finite volume solvers. The models of turbulence Spalart - Allmaras (SU^2)and k-ω SST are used. Inflow turbulence intensity is equal to 5%. Non-dimensional thickness of the first mesh layer y^+ is approximately equal to 1.

Mach number at the channel inlet M_{in} varies from1.2 to 1.4. Figure-6 shows three patterns of shock wave configuration in the channel. If M_{in} increases step-by-step from 1.2 to M_2 the qualitative flow pattern Figure-6 a) with two supersonic regions persists. The distance between the inlet boundary and the shock wave near the wall is denoted by x_s. Meanwhile if M_{in} is further increased, then the supersonic regions coalesce abruptly, and another pattern presented in Figure-6 b) is realized. This pattern have a single supersonic region. There are oblique shocks near the walls. At both sides of oblique shock, the flow is supersonic. In addition, there are three small local subsonic regions. One of them is situated between bow shock and the central body. Others subsonic small regions adjoin to the side surfaces of central body. The between inlet boundary and oblique shock near the wall is denoted by x_s as in the case of two supersonic regions.

Decreasing of inflow Mach number M_{in} from M_2 down to M_1 leads to decreasing of distance x_s and increasing of the size of subsonic regions adjoined to the side surfaces of central body. At $M_{in} = M_1$ the single supersonic region splits into two regions. Therefore, computations reveal a hysteresis in the shock position x_s versus the inflow Mach number M_{in}. In the range of hysteresis, there is a range of Mach number in which asymmetrical solutions exist. The asymmetrical flow pattern is shown in the Figure-6 c). We obtain asymmetrical solution by introducing of asymmetry in the boundary condition at the initial stage of calculation. We started at the angle of attack $\alpha \neq 0$. At the second stage, the obtained solution is used as initial condition.

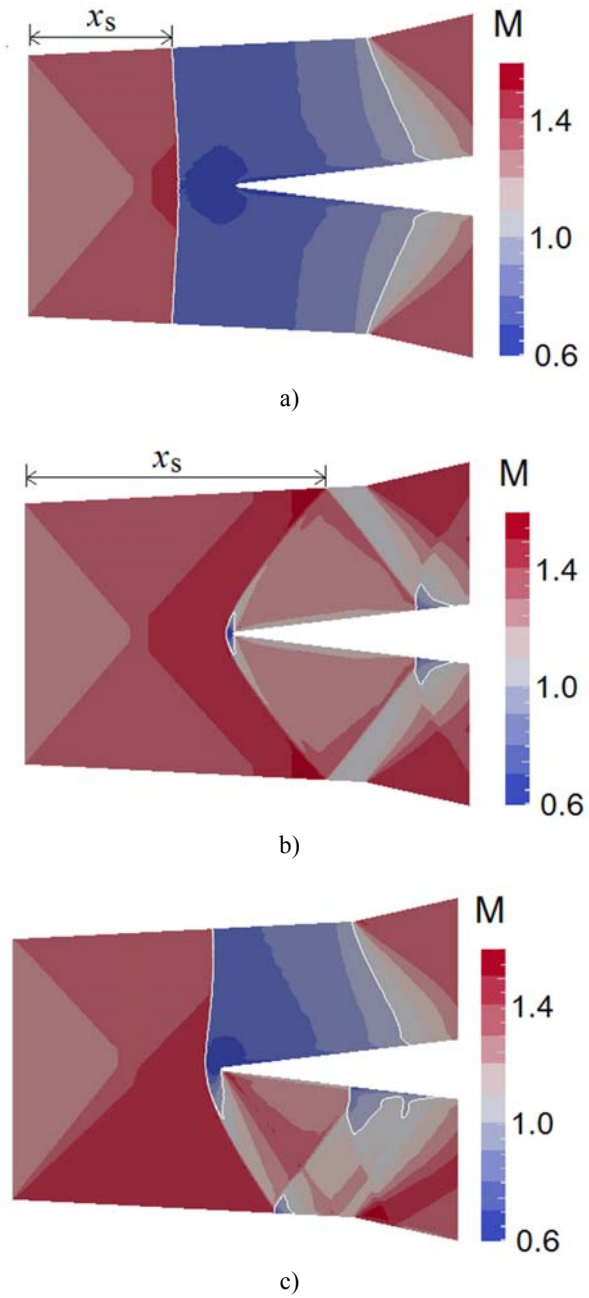

Figure-6. Three patterns of shock wave configuration in the second channel for solutions of Euler equations. $M_{in} = 1.27$. Mach number distribution: a) two supersonic regions, b) single supersonic region,c) asymmetrical solution.

The dependence of distance x_s on inflow Mach number M_{in} is presented in the Figure-7. The range of hysteresis for non-viscous gas is greater than the range of hysteresis for viscous gas. Distance x_s for non-viscous gas is greater than the range of hysteresis for viscous gas.

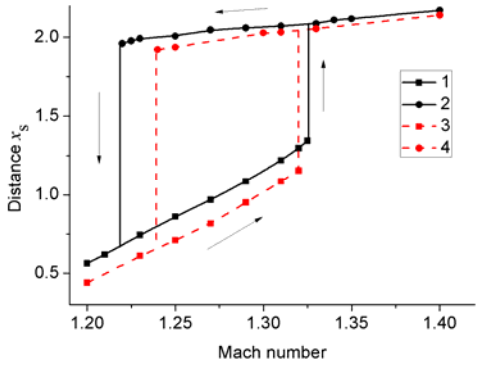

Figure-7. Distance x_s as a function of inflow Mach number M_{in} for second channel. 1, 2 - SU^2 solver, Euler equations, 3, 4 - Ansys CFX solver, RANS equations, turbulence model k-ω SST, $Re = 5.6 \cdot 10^6$. 1, 3 - pattern with two supersonic regions, 2, 4 - pattern with the single region.

Figure-8 shows dependence of x_s on M_{in} for symmetrical patterns (black lines) and asymmetrical ones (red lines).

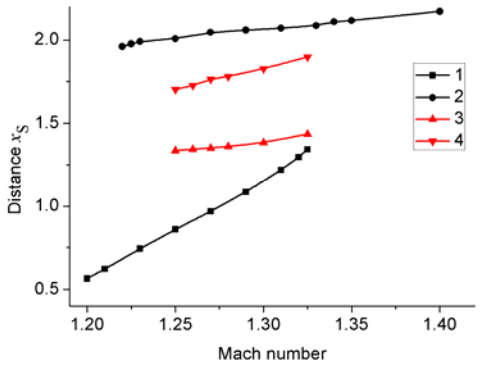

Figure-8. Dependence of distance x_s on inflow mach number for the second channel. Euler equations: 1- pattern with two supersonic regions, 2-pattern with single supersonic region, 3- asymmetrical pattern.

The range of inflow Mach number for asymmetrical patterns is less than hysteresis range. For viscous gas this range is less than the range for non-viscous gas.

Figure-9 demonstrates the hysteresis phenomenon for drag coefficient of central body. Drag coefficient is determined with Ansys CFX for viscous gas at $Re = 3.4 \cdot 10^7$. Figure-9 differs significantly from diagram for the first channel in the Figure-4. If flow pattern is transformed then drag coefficient abruptly changes in both cases of transformation. Drag coefficient of central body in the case of asymmetrical flow pattern is approximately equal to the average drag coefficient for two symmetrical patterns.

The relationship between the lift coefficient and drag coefficient of central body is displayed in the Figure-10. In the Figure-10 there is four separated branches, whose flow patterns differ from one another.

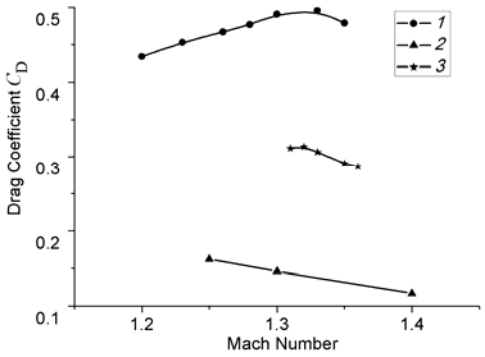

Figure-9. Dependence of drag coefficientC_D of central body in the second channel on inflow Mach number:1-pattern with single supersonic region, 2-patternwith two supersonic regions, 3-asymmetrical pattern.

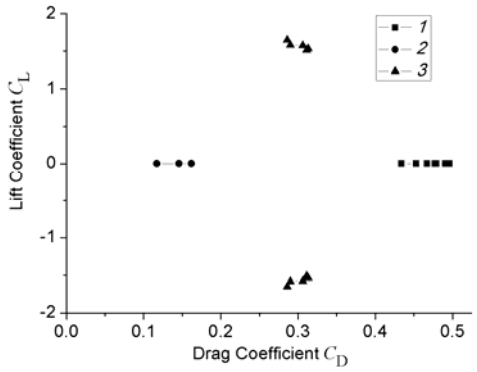

Figure-10. Four regimes of transonic flow in the second channel: 1-single supersonic region, 2-two supersonic region, 3-asymmetrical regimes.

CONCLUSIONS

The numerical simulations of 2D transonic flow in the two channels with central bodies reveal a hysteresis in the shock wave position and in the drag coefficient as the functions of the inflow Mach numbers. The hysteresis range of inflow Mach number for the first channel is less than the range for the second one. It can be explained by existence of long converging parts between channel walls and central body in the second channel. In the certain range of inflow Mach number, there are asymmetrical solutions of the Euler and Reynolds averaged Navier-Stokes equations.

ACKNOWLEDGEMENT

Studies were performed using computing resources providing by "Computing Center of St. Petersburg State University" (http://cc.spbu.ru).

REFERENCES

[1] Ben-Dor G. 2015. Hysteresis phenomena in reflection of shock waves. 29th International Symposium on Shock Waves. Madison. Wisconsin. USA. July 14 19, 2013. Springer. 1: 3-11.

[2] Kudryavtsev A.N., Epstein D.B. 2012. Hysteresis phenomenon of interaction of shock waves generated by a cylinder array. Shock Waves. 22(4): 341-349.

[3] Kudryavtsev A.N., Epstein D.B. 2012. Hysteresis phenomenon in supersonic flow past a system of cylinders. Fluid Dynamics. 47(3): 395-402.

[4] Jameson A. Airfoils admitting non-unique solutions of the Euler equations. 1991. AIAA paper no. 91-1625.

[5] Ivanova A.V, Kuzmin A.G. 2004. Nonuniqueness of the transonic flow past an airfoil. Fluid Dynamics. 39:642-648.

[6] Kuzmin A. 2005. Instability and bifurcation of transonic flow over airfoils. AIAA paper no: 2005-4800.

[7] Kuzmin A. 2009. Bifurcations and buffet of transonic flow past flattened surfaces. Computers & Fluids. 38: 1369-1374.

[8] Kuzmin A. 2012. Non-unique transonic flows over airfoils. Computers and Fluids. 63: 1-8.

[9] Kuzmin A. 2015. Shock wave instability in a channel with an expansion corner. International J. Applied Mechanics. 7(2): 1-9.

[10] Kuzmin A. 2015. Instability of the shock wave/ sonic line interaction. Paris. France. E-print: Centre national de la recherche scientifique. HAL archives, no. 01136894, https://hal.archives-ouvertes.fr/hal-01136894.

[11] Riabinin A., Suleymanov A. 2016. Bifurcation of transonic flow in the channel with a central body. Conference Topical Problems of Fluid Mechanics 2016. Proceedings. 185-190.

[12] Geuzaine Ch., Remacle, J.-F. 2014. Gmsh Reference Manual. University of Liège. Liège. Belgium. 2014. E-print. http://geuz. org/gmsh/doc/texinfo/gmsh.pdf.

[13] Palacios F., Colonno M. R., Aranake A.C., Campos A., Copeland S.R., Economon T.D., Alonso J.J. 2013. Stanford University Unstructured (SU2): An open-source integrated computational environment for multi-physics simulation and design. 51st AIAA Aerospace Sciences Meeting including the New Horizons Forum and Aerospace Exposition. AIAA paper no. 2013-0287. http://su2.stanford.edu/documents/SU2_AIAA_ASM2013.pdf.

[14] ANSYS CFX-Solver Modeling Guide. Release 13.0. 2010. Canonsburg: ANSYS, Inc. p. 604.